HHS Public Access

Author manuscript

Nature. Author manuscript; available in PMC 2013 January 24.

Published in final edited form as:

Nature. 2010 February 18; 463(7283): 968–972. doi:10.1038/nature08766.

Enzyme-inhibitor-like tuning of Ca^{2+} channel connectivity with calmodulin

Xiaodong Liu, **Philemon S. Yang**, **Wanjun Yang**, and **David T. Yue**[‡]

Calcium Signals Laboratory, Departments of Biomedical Engineering and Neuroscience, The Johns Hopkins University School of Medicine, Ross Building, Room 713, 720 Rutland Avenue, Baltimore, MD 21205

Abstract

Ca^{2+} channels and calmodulin are two prominent signaling hubs[1] that synergistically impact functions as diverse as cardiac excitability[2], synaptic plasticity[3], and gene transcription[4]. It is thereby fitting that these hubs are in some sense coordinated, as the opening of Ca_V1-2 Ca^{2+} channels are regulated by a single calmodulin (CaM) constitutively complexed with channels[5]. The Ca^{2+}-free form of CaM (apoCaM) is already preassociated with the IQ domain on the channel carboxy terminus, and subsequent Ca^{2+} binding to this 'resident' CaM drives conformational changes that then trigger regulation of channel opening[6]. Another potential avenue for channel-CaM coordination could arise from the absence of Ca^{2+} regulation in channels lacking a preassociated CaM[6,7]. Natural fluctuations in CaM levels might then influence the fraction of regulatable channels, and thereby the overall strength of Ca^{2+} feedback. However, the prevailing view has been that the ultra-strong affinity of channels for apoCaM ensures their saturation with CaM[8], yielding a significant form of concentration independence between Ca^{2+} channels and CaM. Here, we reveal significant exceptions to this autonomy, by combining electrophysiology to characterize channel regulation, with optical FRET sensor determination of free apoCaM concentration in live cells[9]. This approach translates quantitative CaM biochemistry from the traditional test-tube context, into the realm of functioning holochannels within intact cells. From this perspective, we find that long splice forms of $Ca_V1.3$ and $Ca_V1.4$ channels include a distal carboxy tail[10-12] that resembles an enzyme competitive inhibitor, which retunes channel affinity for apoCaM so that natural CaM variations affect the strength of Ca^{2+} feedback modulation. Given the ubiquity of these channels[13,14], the connection between ambient CaM levels and Ca^{2+} entry via channels is broadly significant for Ca^{2+} homeostasis. Strategies like ours promise key advances for the *in situ* analysis of signaling molecules resistant to *in vitro* reconstitution, such as Ca^{2+} channels.

[‡]Correspondence and requests for materials should be addressed to D.T.Y. voice: (410) 955-0078, fax: (410) 614-8269, (dyue@jhmi.edu).

Author contributions

X.L. devised and refined experimental design; carried out all phases of the experiments; and performed extensive data analysis. P.S.Y. consulted on initial molecular biology approaches; constructed certain channels with ICDI point mutations; and contributed importantly to $Ca_V1.4$ expression strategies and electrophysiological characterization. W.Y. conducted FRET experiments; undertook molecular biology; and extensively managed technical aspects of the project. D.T.Y. conceived, refined, and oversaw the experiments; performed FRET experiments; analyzed data; and wrote the manuscript. All authors commented on and edited the manuscript.

Our investigations build on a $Ca_V1.4$ channel mutation underlying congenital stationary night blindness[15]. This mutation yields a premature stop that deletes the distal carboxy tail (DCT) of these retinal Ca^{2+} channels, and produces a surprising emergence of their Ca^{2+} regulation by CaM[11,12] (Ca^{2+}-dependent inactivation, CDI). Full-length $Ca_V1.4$ channels lack CDI[11,12], thereby maintaining Ca^{2+}-driven transmitter release at tonically depolarized retinal synapses. Hence, the emergence of CDI likely impairs vision. Mechanistically, the DCT contains an ICDI module that is reported to somehow 'switch off' the latent CDI of $Ca_V1.4$ channels[11,12].

Figure 1 summarizes our initial characterization of ICDI effects. Because $Ca_V1.4$ channels yield diminutive currents[16], we appended the DCT of the main $Ca_V1.4$ subunit (α_{1F}) onto the core of better-expressing $Ca_V1.3$ channels (main subunit α_{1D}). This previous approach permits robust investigation of DCT effects[11,12]. As baseline, Fig. 1a displays the CDI of core $Ca_V1.3$ channels (left, $\alpha_{1D\Delta}$), similar to natural short splice variants[8]. Core channels contain all elements required for CDI[6,17], including the IQ domain for apoCaM preassociation[6], and EF-hand-like region for CDI transduction[18]. Depolarization thereby evoked rapidly decaying Ca^{2+} current (middle, red trace), indicative of strong CDI. Since Ba^{2+} binds CaM poorly[17], the slow Ba^{2+} current decay (black trace) delineates the background inactivation of a distinct voltage-dependent process[6,7] (VDI). Thus, the fraction of peak current remaining after 50-msec depolarization (right, r_{50}) relates intimately to inactivation, with the difference between Ca^{2+} and Ba^{2+} r_{50} relations indexing CDI (f_{50}). Appending the $Ca_V1.4$ DCT onto the $Ca_V1.3$ core (Fig. 1b, left) strikingly reduced CDI (middle and right) versus control (dashes) (Supplemental 1.2). Importantly, the DCT did not altogether abolish CDI as reported before[11,12], but spared a clear residuum. This difference foreshadowed major mechanistic and biological consequences.

Hints of these consequences came by qualitative consideration of underlying mechanism. As background, we recapitulated coarse structural underpinnings of DCT effects. To confirm DCT collaboration with core channel elements[11,12], we showed the lack of DCT effects on $Ca_V2.2$ channels (Supplemental 1.3), which presumably lack complementing modules. As well[10,12], only ICDI and A sub-segments (Fig. 1b, left) are required (Supplemental 1.4). Beyond these initial points of clarity, actual DCT mechanisms remain controversial. One group used GST pulldowns of channel peptides to support an allosteric mechanism (Supplemental 1.5), where the ICDI associates with an EF-hand-like module to eliminate CDI transduction[12] (Fig. 1a, left), but leaves apoCaM/channel binding unchanged. By contrast, another group employed channel peptide FRET to advance a competitive mechanism (Supplemental 1.5), where ICDI competes with apoCaM for binding near the channel IQ domain (Fig. 1a, left), thus inhibiting CDI by displacing CaM from channels[11].

To aid resolution, we pursued two preliminary approaches. First, live-cell FRET 2-hybrid assays[6,17] tested whether the $Ca_V1.4$ ICDI (Fig. 2a, CFP fused to ICDI, ECFP–$ICDI_F$) could bind the presumed apoCaM preassociation module of $Ca_V1.3$ (YFP fused to $PreIQ_3$–IQ–A from Fig. 1b, EYFP–$PreIQ_3$–IQ_D–A_F; Supplemental 2.1). We thus resolved a high-affinity *in situ* binding curve (Fig. 2a), where FRET strength (*FR*) is plotted cell-by-cell versus free ECFP–$ICDI_F$ concentration (D_{free}, free donor). By contrast to prior analyses utilizing single-number FRET indices[11], our binding-curve clearly excludes low-affinity interaction, and a

similar binding curve held true for partners solely derived from $Ca_V1.4$ (Supplemental 2.2). We also confirmed avid binding between apoCaM (ECFP–CaM_{WT} in resting cells) and this EYFP–$PreIQ_3$–IQ_D–A_F module[6] (Fig. 2b). More telling, the ICDI (without fluorophore) attenuated the same apoCaM interaction (Fig. 2c, gray zone), suggesting that ICDI and apoCaM could vye for IQ occupancy (Supplemental Fig. 2.2b). In all, these data confirmed the potential for competition, but pertained only to peptides, without guarantee of analogous events within intact channels.

Accordingly, a second provisional approach specifically targeted the holochannel configuration. Scrutiny of mechanisms (Supplemental 1.5) revealed that manipulating apoCaM levels would affect CDI only in the competitive, but not strict allosteric framework. Indeed, elevating CaM sharply reversed ICDI effects (Fig. 2d, middle), and apoCaM chelation eliminated residual CDI (Fig. 2d, right; Supplemental 2.3). Importantly, augmenting CaM also boosted CDI of full-length $Ca_V1.4$ channels (Fig. 2e, cf., ref. 19). Overall, both preliminary approaches supported competition, and the residual CDI seen earlier (Fig. 1b) appeared to reflect incomplete competition. Still, these data neither excluded more nuanced allosteric mechanisms[20], nor revealed whether biologically relevant CaM fluctuations could modulate CDI.

These limitations might be overcome, if only the free apoCaM concentration could be quantified within the very cells where CDI was measured. If so, one could delineate the holochannel equivalent of classic enzyme inhibition plots[20], which rigorously distinguish among mechanisms. Accordingly, we incorporated a recently developed optical FRET-based sensor of apoCaM, $BSCaM_{IQ}$. Here, CFP and YFP flank the apoCaM binding site of neuromodulin[9] (Fig. 3a), such that the overall FRET is determined by free apoCaM concentration. We confirmed the limiting behaviors by coexpressing $BSCaM_{IQ}$ with excess CaM (Fig. 3b, blue line at FR_{min}) or CaM-chelating peptides (green line at FR_{max}; Supplemental 3.1). As expected, *FR* was nearly independent of isolated CFP fluorescence (S_{CFP}), an approximate measure of sensor expression in each cell. By contrast, when $BSCaM_{IQ}$ was expressed alone, *FR* demonstrated a comforting rise towards FR_{max} (Fig. 3b, black line), as anticipated for a sensor that itself chelates and decreases free apoCaM. With reassurance of $BSCaM_{IQ}$ performance in our system, we coexpressed $BSCaM_{IQ}$ and Ca^{2+} channels, and measured free apoCaM concentration before determining CDI in the same cell (Fig. 3c). If free apoCaM were varied among cells by CaM overexpression or chelation, the resulting CDI versus apoCaM plot would rigorously distinguish among mechanisms. Specifically, using the relation between FRET and free apoCaM concentration in our cells[9] (Supplemental 3.2), the exact signature of competition[20] becomes as shown in Fig. 3d (right, gray curves) and

$$CDI = CDI_{max} \cdot \frac{S_b}{S_b \cdot (1-r) + r}; r = K_{dchannelapparent} / K_{dsensor} \quad (1)$$

where CDI_{max} is the maximal CDI without ICDI; $K_{d\text{-channel-apparent}}$ is the apparent dissociation constant of channels for apoCaM (with competitive inhibitor); $K_{d\text{-sensor}}$ is the dissociation constant of $BSCaM_{IQ}$ for apoCaM[9] (2.3 μM); and S_b is the fraction of sensor bound to apoCaM (Supplemental 3.3). As Fig. 3b shows, S_b is directly determined from *FR*,

and ranges from 0 to 1 with increasing apoCaM. If ICDI competition is strong ($r > 1$), curves will be upwardly concave (Fig. 3d, right, gray curves); if weak ($r < 1$), curves will be downwardly concave.

Figure 3d also displays the experimental outcome for core $Ca_V1.3$ channels affixed to the $Ca_V1.4$ DCT ($\alpha_{1D\Delta}$–$(ABI)_F$, from Fig. 1b). In the *CDI*–S_b plot on the right, each symbol corresponds to a single cell, and together these data fit remarkably well to the competitive scheme (red curve, Eq. 1). On the left, current traces from exemplar cells (i, ii, and iii) explicitly demonstrate the appropriate increase of CDI with growing S_b and apoCaM. Importantly, parallel analysis of core $Ca_V1.3$ channels revealed far greater apoCaM affinity (Fig. 3e), yielding maximal CDI throughout. Hence, the upward concavity in Fig. 3d is a genuine ICDI effect, not an unanticipated property of the $Ca_V1.3$ core. Critically, at high apoCaM ($S_b \sim 1$), CDI of both constructs converged, yielding a hallmark of competition[20].

Buoyed by advances for the retinal $Ca_V1.4$ DCT, we wondered whether *CDI*–S_b analysis might uncover like DCT mechanisms in other Ca^{2+} channel subtypes, with yet broader distribution and impact. We considered a long splice variant of the human $Ca_V1.3$ channel[10] ($\alpha_{1D\text{–}long[hum]}$), which contains a DCT homologous to that in $Ca_V1.4$. This long variant has recently been reported to exhibit decreased CDI[10] compared to a short variant akin to core channels (e.g., Fig. 3e). It thus seemed plausible that a competitive ICDI mechanism could extend to these channels, an important possibility given the wide distribution of $Ca_V1.3$ channels[13,14], and the predominance of the long variant throughout brain[10]. Complicating this view, however, were our prior observations that corresponding long and short variants of rat $Ca_V1.3$ channels exhibit no difference in CDI[8]. Indeed, all experiments to this point used the rat $Ca_V1.3$. Accordingly, we undertook *CDI*–S_b analysis of long $Ca_V1.3$ variants from both human and rat. The long $Ca_V1.3$ variant of human (Fig. 3f) clearly adhered to a competitive ICDI mechanism, with maximal CDI equivalent to that of core channels (cf., Fig. 3d). This argues that long forms of $Ca_V1.3$ and $Ca_V1.4$ channels do share a common ICDI mechanism. However, the *CDI*–S_b relation for the long $Ca_V1.3$ variant of humans differs quantitatively from that with the $Ca_V1.4$ DCT (cf., Figs. 3f, d), indicating that the strength of ICDI competition is customized by channel isoform. Indeed, the long $Ca_V1.3$ variant of rat exhibited extreme customization (Fig. 3g). Here, *CDI*–S_b analysis unmasks competitive inhibition, but the competition is weak enough that CDI remains maximal, except with overt chelation of apoCaM (at $S_b \sim 0$). The steep saturation of this *CDI*–S_b relation thus explains prior data that CDI was unaffected by the rat $Ca_V1.3$ DCT, as no depletion was used[8]. Importantly, the *CDI*–S_b curve for the long rat variant (Fig. 3g) is distinct from that for the $Ca_V1.3$ core (Fig. 3e), where CDI stayed maximal throughout. Hence, the rat $Ca_V1.3$ DCT entails customization, not elimination of the competitive inhibitory mechanism (Supplemental 3.4).

The similarity of DCT elements, particularly of human and rat $Ca_V1.3$, suggested that minute differences produce extremes of tuning. Indeed, we found that a single valine-to-alanine switch within the ICDI explains the difference (human:rat, ICDI position 47; Supplemental 3.5).

While the *CDI*–S_b analysis established a competitive inhibitory mechanism at the holochannel level, still critically unresolved was whether the ICDI/IQ peptide interactions studied thus far (Fig. 2c) were relevant to holochannel competition, especially given the multiplicity of CaM sites in channels[6,17,21,22]. This is a generic challenge for large signaling complexes. Importantly, enzyme analysis could be extended to resolve even this ambiguity. Fig. 4a summarizes our data for competitive inhibition in holochannels, recasting *CDI*–S_b data into classic reciprocal-plot form[20], where channel CDI (f_{50}) corresponds to enzyme catalytic velocity *V*, and apoCaM to enzyme substrate *S*. Visual accord with the textbook signature of competition underscores the insights already provided by *in situ* holochannel biochemistry. Beyond this, if ICDI/IQ binding actually underlies holochannel competition, enzyme analysis additionally predicts a linear relation between the apparent apoCaM dissociation constant for holochannels ($K_{\text{d-channel-apparent}}$, Eq. 1) and the reciprocal of the peptide dissociation constant ($1 / K_{\text{d-FRET-peptide}}$)

$$K_{\mathrm{d}channelapparent} = K_{\mathrm{d}channel} \cdot [ICDI] \cdot (1/K_{\mathrm{d}FRETpeptide}) + K_{\mathrm{d}channel} \quad (2)$$

where $K_{\text{d-channel}}$ is the holochannel dissociation constant for apoCaM without inhibitor, and [ICDI] is the effective concentration of ICDI at the channel preassociation site for apoCaM[20] (Supplemental 4.1) Conversely, if peptide interactions are peripheral or the inhibitory mechanism not strictly competitive, this relation will likely fail (Supplemental 4.2). To test this prediction, we noted that *CDI*–S_b analysis had already determined $K_{\text{d-channel-apparent}}$ for channels with three different ICDIs (Figs. 3d, f, g; Fig. 4a). Also, $K_{\text{d-FRET-peptide}}$ for the $Ca_V1.4$ ICDI was measured in Fig. 2a, and the remaining $K_{\text{d-FRET-peptide}}$ values are deduced in Fig. 4b. The resulting linear plot (Fig. 4c) argues that ICDI/IQ binding indeed underlies holochannel competition, and apoCaM/channel preassociation involves the IQ with $K_{\text{d-channel}}$ ~10 nM (Fig. 3e, Supplemental 4.1).

Transforming the reciprocal plots (Fig. 4a) into normal format raises diverse biological implications (Fig. 4d). The dogma has been that Ca^{2+} channels exhibit an ultra-strong apoCaM affinity[8], ensuring maximal CDI over the green biological range[23], as confirmed for channels lacking ICDI (Fig. 4d, gray curve). Earlier reports that ICDI simply 'switches off' CDI[11,12] further promoted this perceived dissociation of CDI and apoCaM fluctuations. By contrast, we show here that the ICDI retunes *CDI*–[apoCaM] relations, so that natural variations of apoCaM modulate CDI and overall Ca^{2+} entry (Fig. 4d). Such interconnection opens new vistas, given the widespread impact and distribution of $Ca_V1.3$ and $Ca_V1.4$ channels[13-15], and the regulation of CaM[23]. For example, coexpressing neuromodulin (a bio-molecule that impacts synaptic growth/remodeling/plasticity and buffers apoCaM[24]) with the long variant of human $Ca_V1.3$ channels indeed lowers apoCaM sufficiently to eliminate CDI and promote Ca^{2+} entry (Fig. 4e, Supplemental 4.3). This outcome may bear on schizophrenia, where hippocampal neuromodulin is decreased[25]. Moreover, neurodegenerative diseases are potentially affiliated with Ca^{2+} dysregulation and thereby altered apoCaM[26]. In Parkinson's, excess alpha-synuclein is pathogenic[27]; these molecules bind apoCaM[28]; and elevated substantia-nigral $Ca_V1.3$ activity predisposes for disease[29]. In Alzheimer's, CaM is depleted[26]. More broadly, certain heart failure models feature elevated CaM[30]. In all, exploring the (patho) physiological sequelae of Ca^{2+} channel connectivity with CaM now beckons at the frontier.

Methods

Molecular biology

Engineering of the rat $Ca_V1.3$ long variant (α_{1D}, AF370009.1) were made as follows. For Fig. 1, a unique XbaI site was introduced by PCR following the IQ domain. The DCT of human α_{1F} (NP005174) was amplified and cloned non-directionally via the unique XbaI site, yielding the sequence in Supplemental 1.1. For Fig. S3.4, a like process was repeated, except appropriate sections of the DCT of rat $Ca_V1.3$ long variant (α_{1D}, AF370009.1) were first PCR amplified with flanking SpeI and XbaI sites (compatible ends), and cloned into the aforementioned unique XbaI site, leaving a unique XbaI site after the inserted section of the rat DCT. Appropriate segments of the ICDI segment of the human $Ca_V1.3$ long variant (α_{1D}, NM000718) were then PCR amplified with flanking SpeI and XbaI sites, and cloned into the unique XbaI site, leaving a unique XbaI site after the inserted ICDI segment. For the V41A insertion (Fig. S3.4d), the human ICDI was point mutated via QuikChange® Mutagenesis (Strategene) prior to PCR amplification and insertion into the channel construct. For the A41V insertion (Fig. S3.4e), the rat ICDI was similar point mutated before cloning into the unique XbaI site of the aforementioned engineered rat $Ca_V1.3$ long variant. For FRET 2-hybrid constructs, fluorophore-tagged CaM constructs were made as described[6]. Other FRET constructs made by replacing CaM with appropriate PCR amplified segments, via unique NotI and XbaI sites flanking CaM[6]. Details of CaM sponges in Supplemental 3.1. All segments subject to PCR or QuikChange® were verified in their entirety by sequencing.

Transfection of HEK293 cells

For electrophysiology experiments, HEK293 cells were cultured in 10 cm plates, and channels were transiently transfected by a calcium phosphate protocol[6,8]. We applied 8 μg of cDNA encoding the desired channel α_1 subunit, along with 8 μg of rat brain β_{2a} (M80545) and 8 μg of rat brain $\alpha_2\delta$ (NM012919.2) subunits. β_{2a} minimized voltage inactivation, enhancing resolution of CDI. Additional cDNA was added as required in co-transfections. All of the above cDNA constructs were driven by a cytomegalovirus promoter. To enhance expression, cDNA for simian virus 40 T antigen (1-2 μg) was co-transfected. For fluorescence resonance energy transfer (FRET) 2-hybrid experiments, transfections and experiments were performed as described[6]. Electrophysiology and FRET were done at room temperature 1–2 d after transfection.

Whole-cell recording

Whole-cell recordings were obtained at room temperature using an Axopatch 200A amplifier (Axon Instruments). Electrodes were pulled with borosilicate glass capillaries (World Precision Instruments, MTW 150-F4), resulting in 1–3 MΩ resistances, before series resistance compensation of 80%. The internal solutions contained, (in mM): $CsMeSO_3$, 135; $CsCl_2$, 5; $MgCl_2$, 1; MgATP, 4; HEPES (pH 7.3), 5; and EGTA, 5; at 290 mOsm adjusted with glucose. The bath solution contained (in mM): TEA-$MeSO_3$, 140; HEPES, 10, pH 7.3; $CaCl_2$ or $BaCl_2$, 10; 300 mOsm, adjusted with glucose. These are as reported[8]. To augment currents for the full-length $Ca_V1.4$ experiments in Fig. 2e, we used 40 mM $CaCl_2$ or $BaCl_2$

in the bath solution, while adjusting TEA-$MeSO_3$ downwards to preserve osmolarity. As well, 5 μM Bay K 8644 was present in the bath throughout to further enhance currents.

FRET optical imaging

FRET 2-hybrid experiments were carried out in HEK293 cells and analyzed as described[6]. During imaging, the bath solution was either a Tyrode's buffer containing 2 mM Ca^{2+}, or the standard electrophysiological recording bath solution described above. Concentration-dependent spurious FRET was subtracted from the raw data prior to binding-curve analysis[17]. For simultaneous $BSCaM_{IQ}$ imaging and patch-clamp recording, three-cube FRET measurements were obtained prior to whole-cell break in, and did not change appreciably thereafter. For ICDI binding curves in Figs. 2a and 4b, unlabelled IQ domain of neuromodulin (sequence in Supplemental 3.1) was coexpressed to reduce interference from endogenous CaM.

Supplementary Material

Refer to Web version on PubMed Central for supplementary material.

Acknowledgments

We thank Michael Tadross, Ivy Dick, and members of the Ca^{2+} signals lab for valuable comments; Michael Tadross for custom and elegant data-acquisition software; D.J. Black and Anthony Persechini for $BSCaM_{IQ}$ and neuromodulin cDNA; J. McRory and Terry Snutch for human α_{1F} cDNA; J. Streissnig for the human α_{1D} cDNA; and Vincent Wu for earlier foundational experiments. Supported by grants from the NIMH (to D.T.Y.), NHLBI (D.T.Y.), and NIDCD (D.T.Y. and Paul Fuchs).

References

1. Jeong H, Tombor B, Albert R, Oltvai ZN, Barabasi AL. The large-scale organization of metabolic networks. Nature. 2000; 407:651–654. [PubMed: 11034217]
2. Alseikhan BA, DeMaria CD, Colecraft HM, Yue DT. Engineered calmodulins reveal the unexpected eminence of Ca^{2+} channel inactivation in controlling heart excitation. Proc Natl Acad Sci U S A. 2002; 99:17185–17190. [PubMed: 12486220]
3. Xu J, Wu LG. The decrease in the presynaptic calcium current is a major cause of short-term depression at a calyx-type synapse. Neuron. 2005; 46:633–645. [PubMed: 15944131]
4. Krey JF, Dolmetsch RE. Molecular mechanisms of autism: a possible role for Ca^{2+} signaling. Curr Opin Neurobiol. 2007; 17:112–119. [PubMed: 17275285]
5. Yang PS, Mori MX, Antony EA, Tadross MR, Yue DT. A single calmodulin imparts distinct N- and C-lobe regulatory processes to individual $Ca_V1.3$ channels. Biophys J. 2007; 92:354a.
6. Erickson MG, Liang H, Mori MX, Yue DT. FRET two-hybrid mapping reveals function and location of L-type Ca^{2+} channel CaM preassociation. Neuron. 2003; 39:97–107. [PubMed: 12848935]
7. Liang H, et al. Unified mechanisms of Ca^{2+} regulation across the Ca^{2+} channel family. Neuron. 2003; 39:951–960. [PubMed: 12971895]
8. Yang PS, et al. Switching of Ca^{2+}-dependent inactivation of $Ca_V1.3$ channels by calcium binding proteins of auditory hair cells. J Neurosci. 2006; 26:10677–10689. [PubMed: 17050707]
9. Black DJ, Leonard J, Persechini A. Biphasic Ca^{2+}-dependent switching in a calmodulin-IQ domain complex. Biochemistry. 2006; 45:6987–6995. [PubMed: 16734434]
10. Singh A, et al. Modulation of voltage- and Ca^{2+}-dependent gating of $Ca_V1.3$ L-type calcium channels by alternative splicing of a C-terminal regulatory domain. The Journal of biological chemistry. 2008; 283:20733–20744. [PubMed: 18482979]

11. Singh A, et al. C-terminal modulator controls Ca^{2+}-dependent gating of $Ca_V1.4$ L-type Ca^{2+} channels. Nat Neurosci. 2006; 9:1108–1116. [PubMed: 16921373]
12. Wahl-Schott C, et al. Switching off calcium-dependent inactivation in L-type calcium channels by an autoinhibitory domain. Proc Natl Acad Sci U S A. 2006; 103:15657–15662. [PubMed: 17028172]
13. Platzer J, et al. Congenital deafness and sinoatrial node dysfunction in mice lacking class D L-type Ca^{2+} channels. Cell. 2000; 102:89–97. [PubMed: 10929716]
14. Namkung Y, et al. Requirement for the L-type Ca^{2+} channel alpha1D subunit in postnatal pancreatic beta cell generation. J Clin Invest. 2001; 108:1015–1022. [PubMed: 11581302]
15. Strom TM, et al. An L-type calcium-channel gene mutated in incomplete X-linked congenital stationary night blindness. Nat Genet. 1998; 19:260–263. [PubMed: 9662399]
16. Doering CJ, Hamid J, Simms B, McRory JE, Zamponi GW. Cav1.4 encodes a calcium channel with low open probability and unitary conductance. Biophys J. 2005; 89:3042–3048. [PubMed: 16085774]
17. Dick IE, et al. A modular switch for spatial Ca^{2+} selectivity in the calmodulin regulation of Ca_V channels. Nature. 2008; 451:830–834. [PubMed: 18235447]
18. Peterson BZ, et al. Critical determinants of Ca^{2+}-dependent inactivation within an EF-hand motif of L-type Ca^{2+} channels. Biophysical Journal. 2000; 78:1906–1920. [PubMed: 10733970]
19. Griessmeier K, et al. Calmodulin is a functional regulator of $Ca_V1.4$ l-type Ca^{2+} channels. J Biol Chem. 2009
20. Cantor, CR.; Schimmel, PR. Biophysical Chemistry: The behavior of biological macromolecules. 11. Macmillan; 1980.
21. Kim J, Ghosh S, Nunziato DA, Pitt GS. Identification of the components controlling inactivation of voltage-gated Ca^{2+} channels. Neuron. 2004; 41:745–754. [PubMed: 15003174]
22. Xiong L, Kleerekoper QK, He R, Putkey JA, Hamilton SL. Sites on calmodulin that interact with the C-terminal tail of Cav1.2 channel. The Journal of biological chemistry. 2005; 280:7070–7079. [PubMed: 15583004]
23. Black DJ, Tran QK, Persechini A. Monitoring the total available calmodulin concentration in intact cells over the physiological range in free Ca^{2+} Cell Calcium. 2004; 35:415–425. [PubMed: 15003851]
24. Slemmon JR, Feng B, Erhardt JA. Small proteins that modulate calmodulin-dependent signal transduction: effects of PEP-19, neuromodulin, and neurogranin on enzyme activation and cellular homeostasis. Mol Neurobiol. 2000; 22:99–113. [PubMed: 11414283]
25. Chambers JS, Thomas D, Saland L, Neve RL, Perrone-Bizzozero NI. Growth-associated protein 43 (GAP-43) and synaptophysin alterations in the dentate gyrus of patients with schizophrenia. Prog Neuropsychopharmacol Biol Psychiatry. 2005; 29:283–290. [PubMed: 15694236]
26. Bezprovanny I. Calcium signaling and neurodegenerative diseases. Trends in Molecular Medicine. 2009; 15:89–100. [PubMed: 19230774]
27. Masliah E, et al. Dopaminergic loss and inclusion body formation in alpha-synuclein mice: implications for neurodegenerative disorders. Science. 2000; 287:1265–1269. [PubMed: 10678833]
28. Lee D, Lee SY, Lee EN, Chang CS, Paik SR. alpha-Synuclein exhibits competitive interaction between calmodulin and synthetic membranes. J Neurochem. 2002; 82:1007–1017. [PubMed: 12358748]
29. Chan CS, et al. 'Rejuvenation' protects neurons in mouse models of Parkinson's disease. Nature. 2007; 447:1081–1086. [PubMed: 17558391]
30. Ikeda S, et al. MicroRNA-1 negatively regulates expression of the hypertrophy-associated calmodulin and Mef2a genes. Mol Cell Biol. 2009; 29:2193–2204. [PubMed: 19188439]

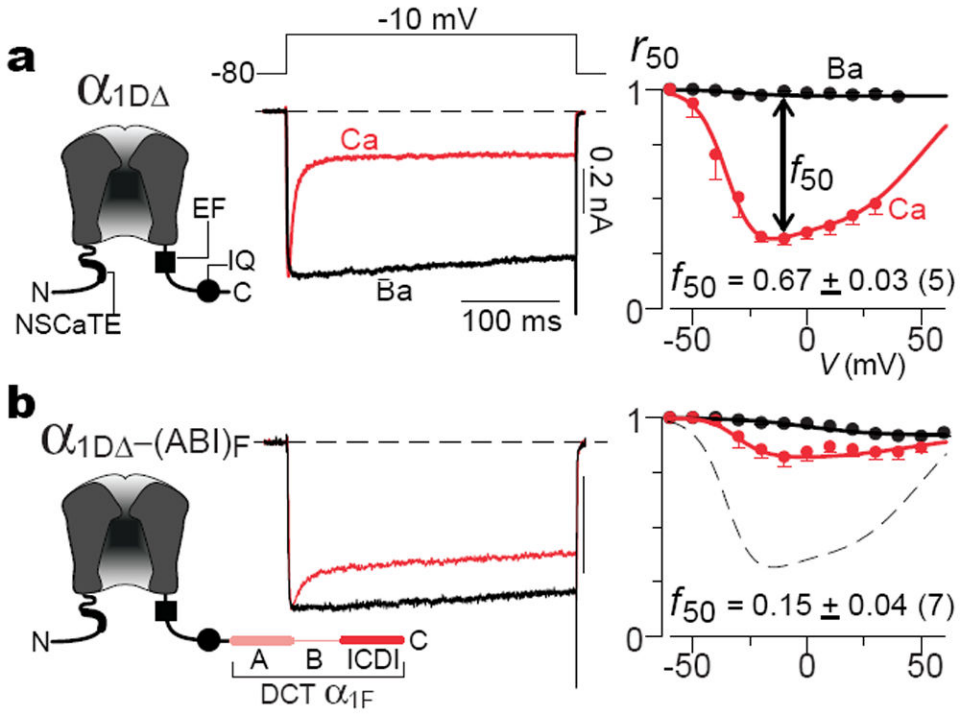

Figure 1. Distal carboxy tail of $Ca_V1.4$ weakens Ca^{2+} regulation of channels

a, Core $Ca_V1.3$ channel contains all known structural elements required for CDI (left schematic of main subunit $\alpha_{1D\Delta}$, containing NSCaTE[17], EF[18], and IQ[6]) and thereby exhibits robust CDI (right two sub-panels). Average f_{50} CDI metric at bottom (mean ± sem), with number of cells in parentheses. Throughout, current bars pertain to Ca^{2+} currents, Ba^{2+} currents scaled for kinetic comparison, and tail currents clipped to frame. **b**, Adding DCT of α_{1F} (main pore-forming $Ca_V1.4$ subunit) to core $Ca_V1.3$ channel weakens CDI. A, B, and ICDI segments of DCT defined in Supplemental 1.1. Dashed curve reproduces baseline from **a**.

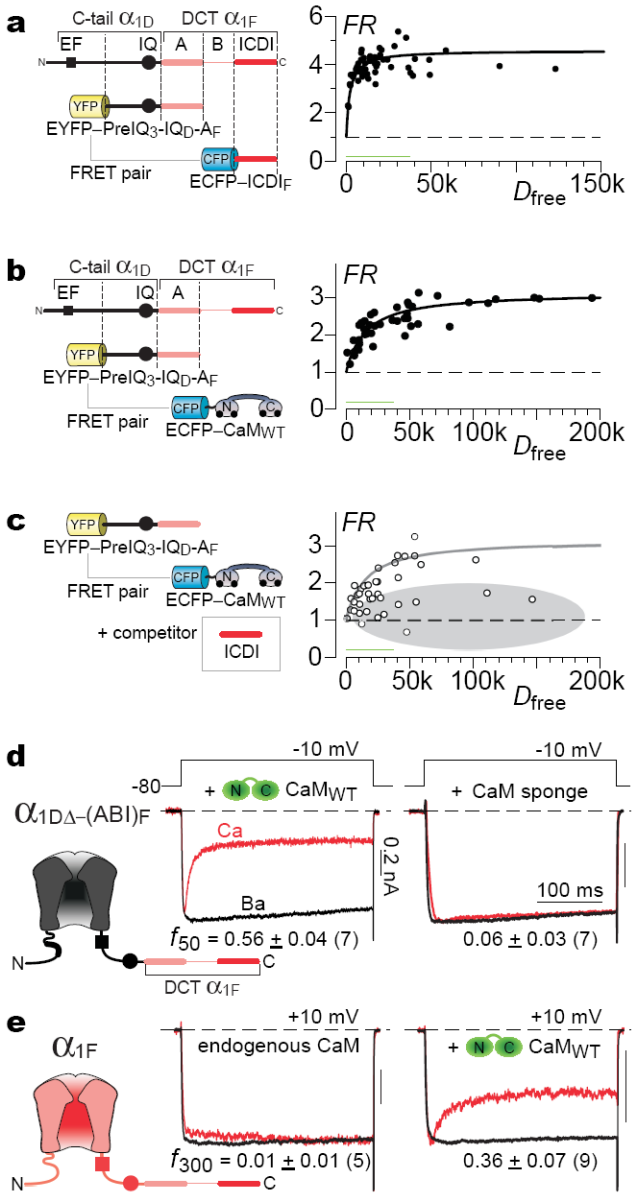

Figure 2. Provisional evidence for competition

a, FRET, CFP-tagged ICDI of α_{1F} versus YFP-tagged PreIQ$_3$-IQ-A from Fig. 1b (Supplemental 2.1). *FR* ∝ FRET efficiency times fraction of YFP-tagged molecules bound[6]. D_{free}, relative concentration of unbound CFP-tagged molecules; green bar ~500 nM[6]. **b**, FRET, apoCaM versus PreIQ$_3$-IQ-A in **a**. **c**, ICDI (without fluorophore) attenuates binding in **b**. Gray reference curve from **b**. **d**, Left, CDI is rescued upon overexpressing CaM with chimera in Fig. 1b. Right, CaM sponge (Ca$_V$1.2 YFP–PreIQ$_3$-IQ[6]) eliminates CDI. **e**, Overexpressing CaM with full-length Ca$_V$1.4. f_{300}, 300-ms version of f_{50}.

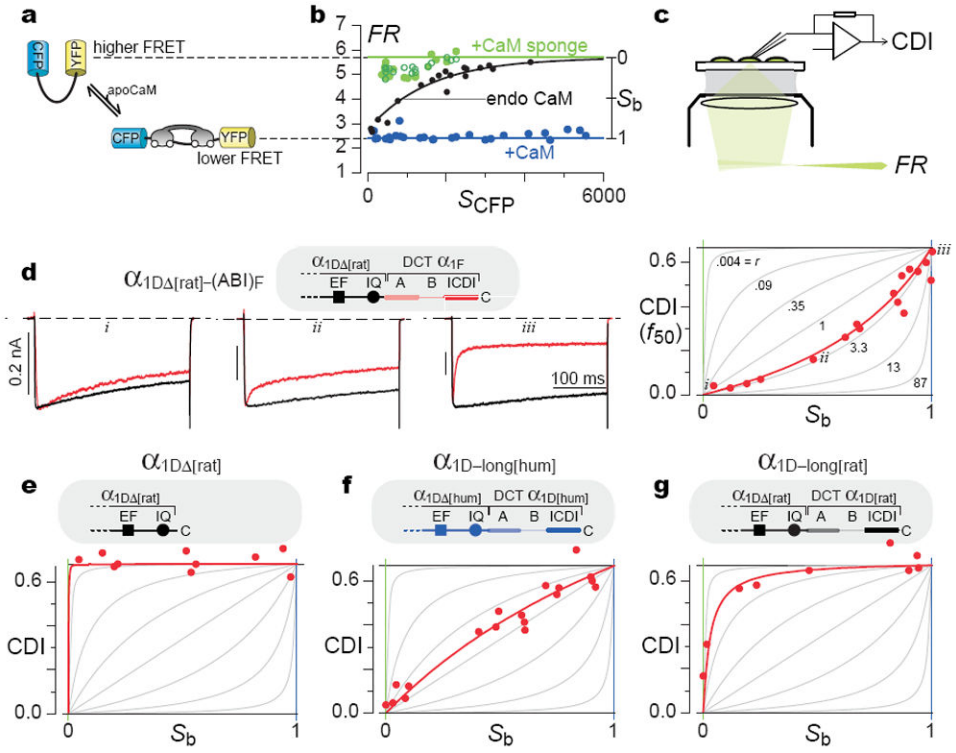

Figure 3. Live-cell holochannel biochemistry proves competition

a, $BSCaM_{IQ}$ schematic. **b**, $BSCaM_{IQ}$ expressed alone (black curve and data), and coexpressed with CaM or CaM sponges (neuromodulin IQ (filled green, Supplemental 3.1) or $Ca_V1.2$ $PreIQ_3$-IQ[6] (open green)). S_{CFP}, isolated CFP fluorescence[6]. **c**, Approach to obtain CDI and FRET readouts of apoCaM (*FR*) in single cells. **d**, *CDI*–S_b analysis for $\alpha_{1D\Delta[rat]}$–$(ABI)_F$, respectively, for -10 mV steps. Right, family of gray *CDI*–S_b curves illustrate potential profiles for competitive inhibition, according to Eq. 1. Superimposed red data and fit conform to competitive profile. Left, corresponding exemplar traces, labelled i-iii. **e-g**, *CDI*–S_b analysis for $\alpha_{1D\Delta[rat]}$, $\alpha_{1D–long[hum]}$, and $\alpha_{1D–long[rat]}$. Format as in **d**.

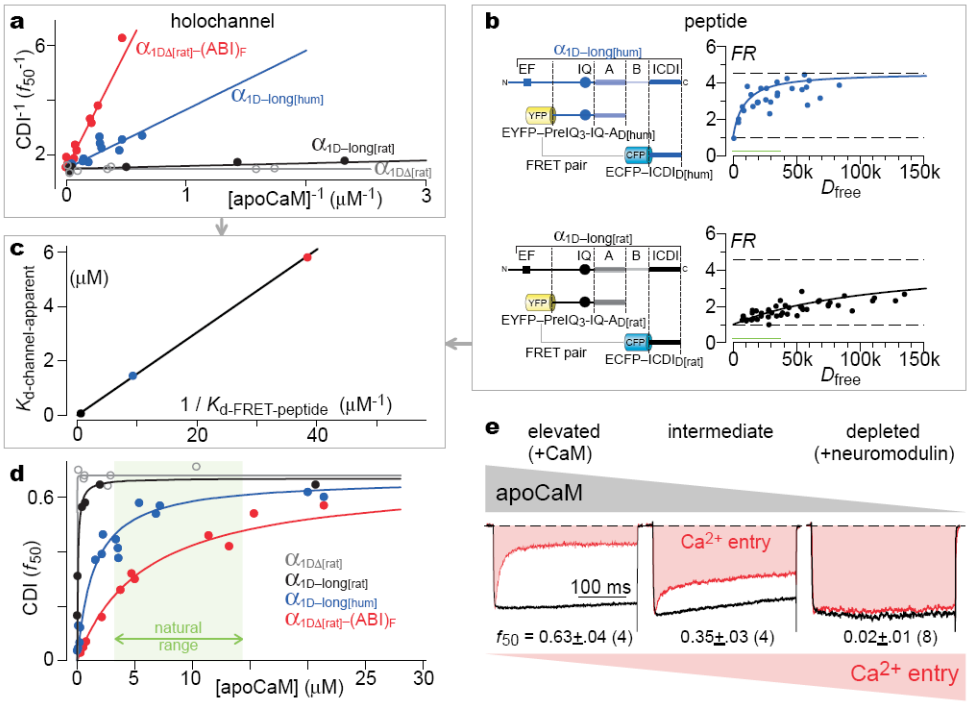

Figure 4. Molecular interactions and biology of competitive inhibitory tuning

a, Reciprocal-plot representation of Fig. 3 (d-g) relations. **b**, FRET assays characterizing presumed peptide interactions underlying holochannel competition (as in **a**). **c**, Linear relation between holochannel and peptide competition parameters. **d**, Linear format of quantitative tuning relations. Green biological range, 99% boundaries[23]. **e**, Consequences of connectivity in long variant of human $Ca_V1.3$. Natural variability of native CaM buffers (neuromodulin) affects CDI and Ca^{2+} entry for long variant of human $Ca_V1.3$. Left, CaM coexpression; middle, endogenous CaM; right, neuromodulin coexpression.